A FINITE ELEMENT METHODOLOGY TO DETERMINE ELASTIC PARAMETERS IN BIOLOGICAL TISSUES

Adair R. Aguiar
Edmar B. T. Prado
Departamento de Engenharia de Estruturas, Escola de Engenharia de São Carlos
Universidade de São Paulo, Av. Trabalhador Sãocarlense, 400, Cx. P. 359
13560-590, São Carlos - SP - Brazil
aguiarar@sc.usp.br
edmarbt@sc.usp.br

Abstract. *Experimental observations reveal that abnormal biological tissues have different mechanical responses from healthy biological tissues. Classical linear elasticity is then used to model the responses of these tissues under small deformations. In particular, soft tissues are modeled as linearly elastic, isotropic, and incompressible materials. The unique determination of the shear elastic modulus, μ, throughout a body is a matter of current research. For a particular class of plane problems, however, it has been shown recently that if μ is known at four different points in a sample, then it can be determined from the knowledge of two displacement fields obtained from two distinct experiments performed on the same sample. This result is used here to propose a finite element methodology to numerically determine μ in a sample of soft tissue, which is subjected to two experiments that can be performed in laboratory. It is assumed that resultant forces are known on complementary parts of the boundary of the sample. No a priori knowledge of the shear elastic modulus is required. The methodology yields numerical results that are both in very good agreement with analytical results and more accurate than numerical results obtained from another methodology presented in the literature.*

Keywords: *Classical Linear Elasticity, Elastography, Hyperbolic Equation, Inverse Problem, Finite Element Method*

1. INTRODUCTION

According to Fung (2004), Ophir et al. (1991), Liu et al. (2003), experimental observations reveal that abnormal biological tissues have different mechanical behavior than normal biological tissues. In particular, Sarvazyan (1993) and Krouskop et al. (1998) oberve that the abnormal tissues are stiffer than the normal tissues. The different behavior observed between the two tissues is used to diagnose the breast cancer. For instance, the exam by touching the patient's breast is still the standard method used by health professionals to determine the presence of lesions in the breast, or, in the prostate. In several cases, however, the lesion may not be detected due to its reduced size, or, due to it localization in deep regions of the body. According to Ophir et al. (2001), the presence of lesions in the interior of the body may not be detected even with the conventional ultrassound exams.

A technique used in Medical Physics to detect the presence of tumors consists of pressing lightly an ultrassonic device on the external surface of the human body, which in turn deforms the part of the body located near this surface. According to Mridha and Ödman (1986) the deformation must be small, less than 2.5 $\%$, so that the viscous behavior of the biological tissue can be ignored and the tissue can be treated as a linear elastic solid.

Park and Maniatty (2006) present a direct inversion approach for reconstructing μ in a nearly incompressible, isotropic, and linearly elastic solid from dynamic measurements of the interior displacement field during time harmonic excitation. The authors use a finite element methodology to find approximate solutions to the governing equations, which does not use boundary conditions. To validate the resulting algorithm, the authors use simulated data with and without noise on a two-dimensional domain. The algorithm is then used to reconstruct μ with magnetic ressonance measured experimental data involving a tissue-mimicking phantom.

In Section 2. we present two distinct classes of plane strain problems in linear elastostatics. First, we consider the *direct problem* of finding the displacement field in an isotropic solid, which is nearly incompresible. Assuming that this field is a good approximation for the displacement field in an incompressible solid, we consider next the *inverse problem* of finding the shear elastic modulus μ and the constraint reaction pressure π in this solid. Assuming that these fields are smooth, we can eliminate π from the equilibrium equations and obtain only one governing equation for μ, which is hyperbolic. The general solution of this equation is given in terms of two arbitrary functions, which can not be determined from the knowledge of one displacement field alone. If, however, two linearly independent displacement fields are known, Barbone and Gokhale (2004) show that the general expression of μ contains at most four arbitray constants. In this work, we assume that these fields are known from two experiments that can be performed in laboratory. We also assume that resultant forces are known on complementary parts of the boundary of the solid. Using these assumptions, we introduce a weak formulation of the inverse problem of finding μ and the constraint reaction pressures in the solid for the two experiments.

In Section 3. we assume that both experiments are performed in a long cylinder of polygonal cross section that is in a state of plane strain deformation perpendicular to his axis and use a standard finite element methodology to construct discrete formulations for the weak version of the direct problem. The experiments are then simulated numerically by solving two discrete direct problems, which yield two linearly independent displacement fields. These solutions also yield resultant forces on complementary parts of the boundary for both experiments. Using both the displacement fields and the data on the boundary, we construct next discrete formulations for the weak version of the inverse problem. The solution of this discrete problem allows the approximate reconstruction of the distribution of μ in the solid.

In Section 4. we introduce the experiments that yield the linearly independent displacement

fields and present numerical results obtained from the solutions of discrete inverse problems. We use color maps to show numerical results that are in very good agreement with the corresponding analytical results. We then compare results obtained in our work with results obtained by Park and Maniatty (2006).

In Section 5. we present some concluding remarks.

2. THE DIRECT AND INVERSE PROBLEMS

In Section 2.1 we present the general statements of both the direct problem, which is used to simulate experiments that can be performed in the laboratory, and the inverse problem, which uses displacement fields obtained from the simulated experiments for the determination of the shear elastic modulus. In Section 2.2 we present the weak formulation of the direct problem and in Section 2.3 we present the weak formulation of the inverse problem.

2.1 The Statements of the Problems

Let $\mathcal{B} \subset \mathbb{R}^2$ be the undistorted natural reference configuration of a body. Points $\mathbf{x} \in \mathcal{B}$ are mapped to points $\hat{\mathbf{x}} \equiv \mathbf{x} + \mathbf{u}(\mathbf{x}) \in \mathbb{R}^2$, where $\mathbf{u}(\mathbf{x})$ is the displacement of $\mathbf{x}$. The boundary $\partial\mathcal{B}$ of $\mathcal{B}$ is composed of two non-intersecting parts, $\partial_1\mathcal{B}$ and $\partial_2\mathcal{B}$, $\partial_1\mathcal{B} \cup \partial_2\mathcal{B} = \partial\mathcal{B}$, $\partial_1\mathcal{B} \cap \partial_2\mathcal{B} = \emptyset$, such that $\mathbf{u}(\mathbf{x}) = \bar{\mathbf{u}}(\mathbf{x})$ for $\mathbf{x} \in \partial_1\mathcal{B}$ and such that a dead load traction field $\bar{\mathbf{t}}(\mathbf{x})$ is prescribed for $\mathbf{x} \in \partial_2\mathcal{B}$.

The body undergoes a small deformation and is in equilibrium in the absence of body force, so that

$$\operatorname{div} \mathbf{T} = \mathbf{0} \quad \text{in } \mathcal{B}\,, \tag{1}$$

where $\mathbf{T}$ is the stress tensor, which must satisfy the loading condition

$$\mathbf{T}\,\mathbf{n} = \bar{\mathbf{t}} \quad \text{on } \partial_2\mathcal{B}\,, \tag{2}$$

with $\mathbf{n}$ being a unit normal to $\partial_2\mathcal{B}$.

We assume that the body is incompressible, isotropic, and linearly elastic, so that $\mathbf{T}$ is given by

$$\mathbf{T} = -\pi\,\mathbf{1} + 2\,\mu\,\mathbf{E}\,, \tag{3}$$

where π is a non-constitutive constraint reaction field, μ is the shear elastic modulus, which depends on the material point $\mathbf{x}$, and

$$\mathbf{E} = \nabla_s \mathbf{u} \equiv \frac{1}{2}\left[\nabla\mathbf{u} + (\nabla\mathbf{u})^T\right] \tag{4}$$

is the infinitesimal strain tensor. Observe from Eq. (3) that $\mathbf{T}$ is determined from both the strain tensor $\mathbf{E}$ and an arbitrary spherical tensor $-\pi\,\mathbf{1}$. For plane problems, any infinitesimal deformation of $\mathcal{B}$ must conserve area, so that

$$\operatorname{tr}\mathbf{E} = \operatorname{div}\mathbf{u} = 0\,. \tag{5}$$

Substituting Eq. (3) into both Eq. (1) and Eq. (2), we obtain

$$-\nabla\,\pi(\mathbf{x}) + 2\,\operatorname{div}(\mu\,\nabla_s\,\mathbf{u})(\mathbf{x}) = \mathbf{0}\,, \qquad \forall\,\mathbf{x} \in \mathcal{B}\,, \tag{6}$$

$$(-\pi + 2\,\mu\,\nabla_s\,\mathbf{u})\;\mathbf{n}\,(\mathbf{x}) = \bar{\mathbf{t}}\,, \qquad \forall\,\mathbf{x} \in \partial_2\mathcal{B}\,, \tag{7}$$

respectively.

The *direct problem* consists of finding both the displacement field $\mathbf{u} : \mathcal{B} \to \mathbb{R}^2$ and the pressure field $\pi : \mathcal{B} \to \mathbb{R}$ that satisfy the kinematic constraint given by Eq. (5) and the equilibrium equation given by Eq. (6) together with the traction condition given by Eq. (7) and the displacement condition $\mathbf{u} = \bar{\mathbf{u}}$ on $\partial_1\mathcal{B}$. If $\partial_1\mathcal{B} = \emptyset$ then the given traction field $\bar{\mathbf{t}}$ must satisfy the usual global equilibrium condition that is essential for the existence of a solution.

The *inverse problem* consists of finding both the shear elastic modulus $\mu : \mathcal{B} \to \mathbb{R}$ and the pressure field $\pi : \mathcal{B} \to \mathbb{R}$ that satisfy the equilibrium equation given by Eq. (6), where $\mathbf{u}$ is known everywhere in $\mathcal{B}$ together with its boundary. Obviously, $\mathbf{u}$ must satisfy the kinematic constraint given by Eq. (5). We assume, however, that the local traction condition given by Eq. (7) is not known, which means that $\partial_1\mathcal{B} = \partial\mathcal{B}$. Barbone and Gokhale (2004) and McLaughlin and Yoon (2004) have shown that, in general, this inverse problem does not have a unique solution. Barbone and Gokhale (2004) have shown, however, that by knowing two linearly independent displacement fields from two experiments performed on the same body in a state of plane strain, the general expression of μ contains at most four arbitrary constants. In Section 3. we use this result together with the assumption that resultant forces are known on complementary parts of the boundary $\partial\mathcal{B}$ in each experiment to determine μ.

2.2 The Weak Formulation of the Direct Problem

Let

$$\mathcal{S} = \{\mathbf{v} : \mathcal{B} \to \mathbb{R}^2 \big| \mathbf{v} \in W^{1,2}(\mathcal{B}), \mathbf{v} = \bar{\mathbf{u}} \text{ a.e. on } \partial_1\mathcal{B}\} \tag{8}$$

be the set of all kinematically admissible displacements and let

$$\mathcal{V} = \{\mathbf{v} : \mathcal{B} \to \mathbb{R}^2 \big| \mathbf{v} \in W^{1,2}(\mathcal{B}), \mathbf{v} = \mathbf{0} \text{ a.e. on } \partial_1\mathcal{B}\} \tag{9}$$

be the set of all admissible variations. Then, a weak formulation of the direct problem stated above consists of determining both $\mathbf{u} \in \mathcal{S}$ and $\pi \in \mathcal{L}^2(\mathcal{B})$ that satisfy

$$\begin{aligned} a_1(\mathbf{u}, \mathbf{v}) - a_2(\pi, \mathbf{v}) &= f(\mathbf{v}), \qquad && \forall\, \mathbf{v} \in \mathcal{V}, \\ a_2(p, \mathbf{u}) &= 0, && \forall\, p \in \mathcal{L}^2(\mathcal{B}), \end{aligned} \tag{10}$$

where

$$a_1(\mathbf{u}, \mathbf{v}) = 2\int_{\mathcal{B}} \mu\, \nabla_s\mathbf{u} \cdot \nabla_s\mathbf{v}\, d\mathbf{x}, \qquad a_2(\pi, \mathbf{v}) = \int_{\mathcal{B}} \pi\ \mathrm{div}\ \mathbf{v}\, d\mathbf{x}, \tag{11}$$

$$f(\mathbf{v}) = \int_{\partial_2\mathcal{B}} \bar{\mathbf{t}} \cdot \mathbf{v}\, \mathbf{dx}. \tag{12}$$

Next, we introduce a penalty formulation of Eq. (10), which yields a simple and efficient numerical procedure to find the solution $(\mathbf{u}, \pi)$ of the direct problem. This formulation is analogous to a penalty formulation used by Aguiar and Fosdick (2000) in the numerical investigation of a class of plane prolems in nonlinear elasticity. In general terms, the *penalty formulation* is based upon relaxing the constraint equation given by Eq. (10.b) and introducing an alternative sequence of problems corresponding to a one-parameter family of *compressible* elastic materials. When the parameter is zero, the constraint equation given by Eq. (10.b) is recovered, and when the parameter is small the solution to the corresponding alternative problem is supposed to be an approximation to the solution $(\mathbf{u}, \pi)$ of Eq. (10).

To implement the penalty formulation, let

$$b(\pi, p) = \frac{1}{2} \int_{\mathcal{B}} \pi \, p \, d\mathbf{x} \,. \tag{13}$$

For $\varepsilon > 0$, consider the problem of finding $\mathbf{u}_\varepsilon \in \mathcal{S}$ and $\pi_\varepsilon \in \mathcal{L}^2(\mathcal{B})$ that satisfy

$$\begin{aligned} a_1(\mathbf{u}_\varepsilon, \mathbf{v}) - a_2(\pi_\varepsilon, \mathbf{v}) \quad &= f(\mathbf{v}) \,, \qquad && \forall \, \mathbf{v} \in \mathcal{V} \,, \\ \varepsilon \, b(\pi_\varepsilon, p) + a_2(p, \mathbf{u}_\varepsilon) \quad &= \quad 0 \,, \qquad && \forall \, p \in \mathcal{L}^2(\mathcal{B}) \,, \end{aligned} \tag{14}$$

where the penalty parameter $\varepsilon > 0$ is sufficiently small. By using Eq. (13) and eliminating $\pi_\varepsilon(\cdot)$ from the system given by Eq. (14), the alternative problem reduces to determining $\mathbf{u}_\varepsilon \in \mathcal{S}$ such that

$$a_1(\mathbf{u}_\varepsilon, \mathbf{v}) + c(\mathbf{u}_\varepsilon, \mathbf{v}) = \, f(\mathbf{v}) \,, \qquad \forall \, \mathbf{v} \in \mathcal{V} \,, \tag{15}$$

where

$$c(\mathbf{u}_\varepsilon, \mathbf{v}) = \frac{2}{\varepsilon} \int_{\mathcal{B}} (\operatorname{div} \mathbf{u}_\varepsilon)(\operatorname{div} \mathbf{v}) \, d\mathbf{x} \,. \tag{16}$$

We then want to find $\mathbf{u}_\varepsilon \in \mathcal{S}$ that satisfies the Eq. (15), where $a_1(\cdot, \cdot)$, $f(\cdot)$, and $c(\cdot, \cdot)$ are given by, respectively, Eq. (11.a), Eq. (12), and Eq. (16). It is well known that for $\varepsilon > 0$ and $\mu > 0$, this problem has a unique solution $(\mathbf{u}_\varepsilon, \pi_\varepsilon) \in \mathcal{S} \times \mathcal{L}^2(\mathcal{B})$ that converges to the solution $(\mathbf{u}, \pi)$ of Eq. (10) as $\varepsilon \to 0$.

The penalty formulation for the direct problem stated above is equivalent to the weak formulation of the boundary value problem for a compressible, isotropic, and linearly elastic solid. To see this, introduce

$$\mathbf{T} = \lambda \, \operatorname{div} \mathbf{u} \, \mathbf{1} + 2 \, \mu \, \nabla_s \mathbf{u} \tag{17}$$

into both Eq. (1) and Eq. (2), where λ is a Lamé modulus, and consider the weak formulation of the corresponding direct problem, which consists of determining $\mathbf{u} \in \mathcal{S}$ that satisfies

$$a(\mathbf{u}, \mathbf{v}) - f(\mathbf{v}) = 0 \,, \qquad \forall \, \mathbf{v} \in \mathcal{V} \,, \tag{18}$$

where $f(\mathbf{v})$ is given by Eq. (12) and

$$a(\mathbf{v}, \mathbf{v}) = \int_{\mathcal{B}} \left(\lambda \, \operatorname{div} \mathbf{u} \, \operatorname{div} \mathbf{v} + 2 \, \mu \, \nabla_s \mathbf{u} \cdot \nabla_s \mathbf{v} \right) \, d\mathbf{x} \,. \tag{19}$$

Thus, if we consider that λ in Eq. (19) is constant and equal to $2/\varepsilon$ in Eq. (16), then both formulations are equivalent.

2.3 The Weak Formulation of the Inverse Problem

Recall from Section 2.1 that the inverse problem consists of finding both the shear elastic modulus $\mu : \mathcal{B} \to \mathbb{R}$ and the pressure field $\pi : \mathcal{B} \to \mathbb{R}$ that satisfy the equilibrium equation in Eq. (6), where $\mathbf{u}$ satisfies the kinematic constraint given by Eq. (5). We assume that $\mathbf{u} \in \mathcal{W}^{1,2}(\mathcal{B})$ is known and that $\partial_2 \mathcal{B} = \emptyset$. It follows from our discussion of the inverse problem in Section 2.1 that the solution of this problem can not be determined from only one displacement field and that we need two displacement fields $\mathbf{u}^1$ and $\mathbf{u}^2$, obtained from two different

experiments, to determine μ up to four constants. In this work, we assume that these two fields are known, which implies that both $\mathbf{u}^1$ and $\mathbf{u}^2$ satisfy the Eq. (10.b) identically.

In addition, we assume that resultant forces are known on r complementary parts of $\partial\mathcal{B}$. These forces are given by

$$\mathbf{R}_i^j = \int_{\partial_i\mathcal{B}} \mathbf{T}^j\,\mathbf{n}_i\,d\mathbf{x}\,, \qquad i=1,\ldots,r\,, \quad j=1,2\,, \tag{20}$$

where $\partial\mathcal{B} \equiv \bigcup_{i=1}^{r} \partial_i\mathcal{B}$, $\partial_i\mathcal{B}\bigcap\partial_j\mathcal{B}=\emptyset$ for $i\neq j$, and $\mathbf{n}_i$ is the unit normal to $\partial_i\mathcal{B}$. Also, the stress fields $\mathbf{T}^1$ and $\mathbf{T}^2$ are related to the displacement fields $\mathbf{u}^1$ and $\mathbf{u}^2$, respectively, through linear constitutive relations of the form given by Eq. (3). Here, these forms are given by

$$\mathbf{T}^j = -\pi^j\,\mathbf{1} + 2\,\mu\,\nabla_s\mathbf{u}^j\,, \qquad j=1,2\,, \tag{21}$$

where π^j is the constraint reaction field corresponding to the j^{th} experiment. Obviously, $\sum_{i=1}^{r}\mathbf{R}_i^j = \mathbf{0}$ for $j=1,2$.

Since $\partial_2\mathcal{B}=\emptyset$, we set $\partial_1\mathcal{B}=\partial\mathcal{B}$ in both Eq. (8) and Eq. (9). Also, it follows from Eq. (12) that $f(\mathbf{v})=0$ in (10.a).

We now replace $\mathbf{u}$ in both Eq. (10.a) and Eq. (11.a) by either $\mathbf{u}^1$ or $\mathbf{u}^2$. The weak form of the inverse problem that we shall consider in this work consists of finding $\mu\in\mathcal{L}^2(\mathcal{B})$ and $\pi^j\in\mathcal{L}^2(\mathcal{B})$, $j=1,2$, that satisfy

$$-\int_{\mathcal{B}}\pi^j\;\text{div}\;\mathbf{v}\,d\mathbf{x} + 2\int_{\mathcal{B}}\mu\,\nabla_s\mathbf{u}^j\cdot\nabla_s\mathbf{v}\,d\mathbf{x} = 0\,, \qquad j=1,2\,, \qquad \forall\,\mathbf{v}\in\mathcal{V}\,, \tag{22}$$

together with both Eq. (20) and Eq. (21).

3. THE DISCRETE FORMULATIONS

We want to construct approximations to the solution $(\mathbf{u}_\varepsilon,\pi_\varepsilon)\in\mathcal{S}\times L^2(\mathcal{B})$ of the direct problem, given by (15) together with Eq. (11.a), Eq. (12), and Eq. (16), for a given $\varepsilon>0$ and to the solution $(\mu,\pi^1,\pi^2)\in\mathcal{L}^2(\mathcal{B})\times\mathcal{L}^2(\mathcal{B})\times\mathcal{L}^2(\mathcal{B})$ of the inverse problem, given by Eq. (22) together with Eq. (20) and Eq. (21). For this, we consider a Finite Element formulation based on the introduction of discrete problems over finite-dimensional subsets of $\mathcal{S}$, given by Eq. (8), $\mathcal{V}$, given by Eq. (9), and $\mathcal{L}^2(\mathcal{B})$. The corresponding discrete problems can be solved using direct solvers, as opposed to iterative solvers used in the literature[1].

We begin by assuming that $\mathcal{B}\subset\mathbb{R}^2$ is a polygonal domain composed of m non-overlapping quadrilaterals $\mathcal{K}_i\in\mathbb{R}^2$, so that

$$\mathcal{B} = \bigcup_{i=1}^{m}\mathcal{K}_i\,, \tag{23}$$

and such that the intersection of any two of these quadrilaterals is either empty, a point, or, a straight line. For each $\mathcal{K}_i\subset\mathcal{B}$, the interior of the quadrilateral $\mathcal{K}_i$ is non empty.

Let $\mathcal{K}_i$, $i=1,\ldots,m$, be endowed with the set of nodes $\{\mathbf{x}_{ik}\in\mathcal{K}_i,\ k=1,\ldots,4\}$, which are the vertices of $\mathcal{K}_i$. We shall consider *Lagrange finite elements* $(\mathcal{K}_i,\mathcal{P}_i,\Sigma_i)$, $i=1,\ldots,m$, where $\mathcal{P}_i$ is a set of smooth functions $\varphi:\mathcal{K}_i\to\mathbb{R}$ and Σ_i is a set of degrees of freedom

[1] See, for instance, references cited in Park and Maniatty (2006).

corresponding to the coefficients $\varphi(\mathbf{x}_{ik})$. The functions φ are linear combinations of normalized basis functions $\varphi_{ik},\ k = 1, \ldots,\ 4$, so that $\varphi_{ik}(\mathbf{x}_{il}) = \delta_{kl},\ k,\ l = 1,\ \ldots,\ 4$. The functions φ_{ik} are continuous over $\mathcal{K}_i$. In this way, a *finite element mesh* is the union of all the finite elements $(\mathcal{K}_i, \mathcal{P}_i, \Sigma_i)$.

Let us denote as $\mathcal{N} = \{\mathbf{x}_1, \ldots, \mathbf{x}_n\} \subset \bar{\mathcal{B}}$ the complete set of n nodes in $\bar{\mathcal{B}}$. Then, for each $i = 1, \ldots, m$ and each $k = 1, \ldots, 4$, $\mathbf{x}_{i\,k} \in \mathcal{K}_i$ corresponds to a unique element from $\mathcal{N}$. We define the set of functions $\{\varphi_j : \mathcal{B} \to \mathbb{R}\,, j = 1, \ldots, n\}$, such that $\varphi_j(\mathbf{x}) = \varphi_{ik}(\mathbf{x})$ for $\mathbf{x} \in \mathcal{K}_i$, $j = 1, \ldots, n$, $k = 1, \ldots, 4$. Thus, φ_j is continuous on $\mathcal{B}$ and satisifies $\varphi_j(\mathbf{x}_i) = \delta_{j\,i}$. In fact, the set of functions φ_j is a finite dimensional basis for the set of continuous functions defined by

$$\mathcal{P} = \left\{ \varphi : \mathcal{B} \to \mathbb{R} | \varphi(\mathbf{x}) = \sum_{j=1}^{n} \alpha_j\, \varphi_j(\mathbf{x})\,, (\alpha_1, \ldots, \alpha_n) \in \mathbb{R}^n \right\}\,. \tag{24}$$

3.1 The Discrete Direct Problem

We now define the finite dimensional space $\mathcal{V}_h$ as follows

$$\mathcal{V}_h = \{\mathbf{v} : \mathcal{B} \to \mathbb{R}^2 \big| \mathbf{v} \in \mathcal{P} \times \mathcal{P}\,,\ \mathbf{v} = 0 \text{ on } \partial_1\mathcal{B}\}\,, \tag{25}$$

where h stands for the characteristic length of the finite element mesh. Since Eq. (23) holds by assumption, we note that $\mathcal{V}_h \subset \mathcal{V}$. A function $\mathbf{v} \in \mathcal{V}_h$ has the representation

$$\mathbf{v}(\mathbf{x}) = \sum_{i=1}^{2\,n} \vartheta_i \mathbf{w}_i(\mathbf{x}), \qquad \mathbf{x} \in \bar{\mathcal{B}} \equiv \mathcal{B} \cup \partial\mathcal{B}\,, \tag{26}$$

where $\vartheta_i \in \mathbb{R}$, and $\mathbf{w}_i$ is a vector in $\mathbb{R}^2$ of the form

$$\mathbf{w}_{2j-1} = (\varphi_j, 0)\,, \qquad \text{and} \qquad \mathbf{w}_{2j} = (0, \varphi_j)\,, \qquad j = 1, \ldots, n\,, \tag{27}$$

relative to a fixed orthonormal base, with φ_j being a scalar basis function defined for the j^{th} node in the set $\mathcal{N}$ defined above.

In particular, notice that $\mathbf{v}(\mathbf{x}_i) = (\vartheta_{2i-1}, \vartheta_{2i})$ for $i = 1, \ldots, n$. Each $\vartheta_i,\ i = 1, \ldots, 2\,n$, is a *degree of freedom associated with* $\mathcal{V}_h$. Thus, considering the fact that each node in $\mathcal{N}$ has two degrees of freedom and that $\mathbf{v} \in \mathcal{V}_h$, it is convenient to decompose the complete set of $2\,n$ degrees of freedom into two complementary integer sets $\mathcal{Z}^*$ and $\mathcal{Z}$ such that $\vartheta_i = 0\,,\ \forall\, i \in \mathcal{Z}^*$ and $\mathcal{Z} \equiv \{1, 2, \ldots, 2\,n\} \backslash \mathcal{Z}^*$.

Similar to the set $\mathcal{V}_h$, we also introduce the set $\mathcal{S}_h$ defined by

$$\mathcal{S}_h = \{\mathbf{u} : \mathcal{B} \to \mathbb{R}^2 \big| \mathbf{u} \in \mathcal{P} \times \mathcal{P}\,, \mathbf{u} = \bar{\mathbf{u}} \text{ on } \partial_1\mathcal{B}\}\,. \tag{28}$$

Observe that a displacement $\mathbf{u} \in \mathcal{S}_h$ has the representation

$$\mathbf{u}(\mathbf{x}) = \sum_{i=1}^{2\,n} \upsilon_i \mathbf{w}_i(\mathbf{x})\,, \tag{29}$$

where, for each index $i \in \mathcal{Z}^*$, the corresponding value of υ_i is prescribed, $\upsilon_i = \bar{\upsilon}_i$.

Let us also define the space

$$\mathcal{L}_h^2 = \{p : \mathcal{B} \to \mathbb{R} \big|\ p \text{ is piecewise continuous on } \mathcal{B}\}\,. \tag{30}$$

An element $p \in \mathcal{L}^2_h$ has the representation

$$p(\mathbf{x}) = \sum_{i=1}^{m} p_i \tau_i(\mathbf{x}) \,, \qquad \mathbf{x} \in \bar{\mathcal{B}}, \tag{31}$$

where $p_i \in \mathbb{R}$ and τ_i is a scalar basis function, which is piecewise constant, has support in $\mathcal{K}_i$, and is normalized so that $\tau_i(\mathbf{x}) = \delta_{ij}$ for $\mathbf{x} \in \mathcal{K}_j$, $i, j = 1, \ldots, m$.

Now, for a given penalty parameter $\varepsilon > 0$, we substitute both $\mathbf{u}_\varepsilon$, of the form given by Eq. (29), and $\mathbf{v}$, given by Eq. (26), into Eq. (11.a), Eq. (12), and Eq. (16). Since the coefficients $\vartheta_i \,, i \in \mathcal{Z}$, are arbitrary, we can rewrite Eq. (15) in the form

$$\sum_{j=1}^{n} \left(\kappa_{i\,j} + \hat{\kappa}_{i\,j}\right) \upsilon_i = \gamma_i \,, \qquad i \in \mathcal{Z} \,, \tag{32}$$

where

$$\kappa_{i\,j} = a_1(\mathbf{w}_i, \mathbf{w}_j) \,, \qquad \hat{\kappa}_{i\,j} = c(\mathbf{w}_i, \mathbf{w}_j) \,, \tag{33}$$

$$\gamma_i = f(\mathbf{w}_i) \,, \tag{34}$$

The *discrete direct problem* associated to the space $\mathcal{V}_h$ and obtained from the penalty formulation in Eq. (15) consists of finding the coefficients $\upsilon_i \,, i \in \mathcal{Z}$, in $\mathbf{u}_{\varepsilon h} \equiv \sum_{i=1}^{2\,n} \upsilon_i \mathbf{w}_i(\mathbf{x}) \in \mathcal{V}_h$, that satisfy the linear system given by Eq. (32) together with Eq. (33) and Eq. (34). Recall from Section 2. that, for the direct problem, both μ in Eq. (11) and ε in Eq. (16) are known and $\partial_2\mathcal{B}$ may not empty.

Holding h fixed and decreasing ϵ, we generate a sequence of solutions parameterized by ϵ for the discrete problem that converges to a limit function $\mathbf{u}_h$. We then refine the Finite Element mesh by decreasing h and repeat the process above. In so doing, we generate a sequence of solutions $\mathbf{u}_h$ parameterized by h which converges to the solution $\mathbf{u}$ of the original problem given by Eq. (10) together with Eq. (11) and Eq. (12).

3.2 The Discrete Inverse Problem

We use the discrete formulation presented in Section 3.2 to simulate numerically the two experiments that yield the displacement fields $\mathbf{u}^1$ and $\mathbf{u}^2$ that are required for the determination of μ, as described in Section 2.3. The resultant forces $\mathbf{R}^1_i$ and $\mathbf{R}^2_i$ acting on complementary parts $\partial_j\mathcal{B}$ of $\partial\mathcal{B}$ are then evaluated from Eq. (20) together with Eq. (21), where an approximation for π^j is obtained from Eq. (14.b) and is given by

$$\pi^j = \frac{2}{\varepsilon} \, \mathrm{div}\, \mathbf{u}^j \,, \qquad j = 1, 2 \,. \tag{35}$$

We observe from Section 3.1 that $\partial_2\mathcal{B}$ might not be empty. In this section, $\partial_2\mathcal{B} = \emptyset$, which yields a decomposition of the complete set of $2\,n$ degrees of freedom into two complementary integer sets $\mathcal{Z}^*_I$ and $\mathcal{Z}_I$ such that $\vartheta_i = 0 \,, \forall\, i \in \mathcal{Z}^*_I$ and $\mathcal{Z}_I \equiv \{1, 2, \ldots, 2\,n\} \backslash \mathcal{Z}^*_I$. Although similar to the definition of $\mathcal{Z}^*$ in 3.1, it is evident from the previous observation that the definition of $\mathcal{Z}^*_I$ implies that $\mathcal{Z}^* \subseteq \mathcal{Z}^*_I$.

Next, we assume that both fields $\mathbf{u}^1$ and $\mathbf{u}^2$ are known and use the representation given by Eq. (31) to approximate μ and π^j, $j = 1, 2$, in the form

$$\mu(\mathbf{x}) \approx \mu_h(\mathbf{x}) \equiv \sum_{i=1}^{m} \mu_i \tau_i(\mathbf{x}) \,, \qquad \pi^j(\mathbf{x}) \approx \pi^j_h(\mathbf{x}) \equiv \sum_{i=1}^{m} \pi^j_i \tau_i(\mathbf{x}) \,, \qquad \mathbf{x} \in \bar{\mathcal{B}} \,, \tag{36}$$

where $\mu_i \in \mathbb{R}$ and $\pi_i^j \in \mathbb{R}$, $j = 1, 2$. We also assume that $\partial_j \mathcal{B} \subset \partial\mathcal{B}$ is given by

$$\partial_j \mathcal{B} = \bigcup_{p \in \mathcal{Z}_j} \mathcal{D}_p \,,$$

where $\mathcal{D}_p$ is a side of $\mathcal{K}_p$ that belongs to $\partial_j \mathcal{B}$ and $\mathcal{Z}_j$ is the set of integer numbers that identify the finite elements with sides contained in $\partial_j \mathcal{B}$.

Substituting the Eq. (36) and $\mathbf{v}$, given by Eq. (26), into Eq. (20) - Eq. (22), and using the fact that the coefficients $\vartheta_i \,, i \in \mathcal{Z}$, are arbitrary, these expressions can be rewritten as

$$\begin{aligned} \sum_{q=1}^{2\,m} \alpha_{p\,q}^j \omega_q^j &= 0 \,, \qquad p \in \mathcal{Z}_I \,, \\ \sum_{q \in \mathcal{Z}_i} \beta_q^j \omega_q^j &= \mathbf{R}_i^j \,, \qquad i = 1, 2, \ldots, r \,, \end{aligned} \tag{37}$$

where $j = 1, 2$ and

$$\begin{gathered} \alpha_{p\,(2\,q-1)}^j = 2 \int\limits_{\mathcal{K}_q} \nabla_s \mathbf{u}^j \cdot \nabla_s \mathbf{w}_p \, d\,\mathbf{x} \,, \qquad \alpha_{p\,(2\,q)}^j = -\int\limits_{\mathcal{K}_q} \operatorname{tr} \nabla_s \mathbf{w}_p \, d\,\mathbf{x} \,, \\ \beta_{2\,q-1}^j = 2 \int\limits_{\mathcal{D}_q} \left(\nabla_s \mathbf{u}^j\right) \mathbf{n}_q \, d\,\mathbf{x} \,, \qquad \beta_{2\,q}^j = -\int\limits_{\mathcal{D}_q} \mathbf{n}_q \, d\,\mathbf{x} \,, \\ \omega_{2\,q-1}^j = \mu_q \,, \qquad \omega_{2\,q}^j = \pi_q^j \,. \end{gathered} \tag{38}$$

Then, the *discrete inverse problem* associated to the problem given by Eq. (20) and Eq. (21) consists of finding the coefficients $\omega_q^j \,, j = 1, 2 \,, q = 1, \ldots, m$, defined by (38.c) that satisfy the linear system given by Eq. (37) together with Eq. (38.a,b).

In general, the linear system of Eq.(37) together with Eq. (38) is over-determined. To solve this system, we use the Singular Value Decomposition algorithm presented by Golub and van Loan (1996). The main input data are the coefficients on the right side of Eq. (37.a, b), the matrix $\mathbf{W}$ formed by the coefficients that multiply ω_q^j, the dimensions of $\mathbf{W}$, and a tolerance that yields the largest non-singular, square matrix of $\mathbf{W}$. Here, the tolerance is a non-negative number below which a singular value of $\mathbf{W}$ is considered zero. A preliminary study of the influence of the tolerance on the values of the coefficients $\mu_i \,, i = 1, \ldots, m$ in Eq. (36) allows to conclude that, for tolerances below 10^{-8}, all the values obtained for these coefficients were physically plausible and differed very little from each other.

4. NUMERICAL RESULTS

We use the discrete formulations introduced in Section 3. to obtain the shear elastic modulus μ of a long cylinder that is in a state of plane strain parallel to its bases. For this, recall from Section 2. that we need two displacement fields obtained from two distinct experiments performed on this cylinder. In this work, we simulate numerically the two experiments. We assume that the cylinder has a square cross section and contains a cylindrical inclusion of circular cross section, as illustrated in Fig. 1. The sides of the square section have length $\bar{\xi} = 50$ mm and the radius of the circular inclusion is $\bar{\rho} = 6$ mm. Both the cylinder without the inclusion, which we call the *matrix*, and the inclusion itself are homogeneous and nearly incompressible, with elastic constants given by

$$\nu_M = 0,499999 \,, \qquad \mu_M = 36000\,\text{Pa} \,, \qquad \nu_I = \nu_M \,, \qquad \mu_I = C_R\,\mu_M \,, \tag{39}$$

where ν is the Poisson ratio and the sub-indices M and I denote, respectively, the matrix and the inclusion. Also, $C_R \geq 0$ is the shear modulus constrast ratio, so that $C_R = 0$ corresponds to an empty hole, $C_R = 1$ corresponds to a homogeneous cylinder, and $C_r > 1$ corresponds to an inclusion that is C_R times stiffer than the matrix.

Since $\lambda = 2\,\mu\nu/(1-2\,\nu)$ and $\lambda = 2/\varepsilon$ from the discussion about the penalty formulation at the end of Section 2.2, the expressions for ν in Eq. (39) yield penalty parameters for the matrix and the inclusion that are of the order 10^{-11}. We have verified that the results shown in this work are not sensitive to the choice of $\nu_M = \nu_i$ in Eq. (39), as long as this choice is very close to 0.5.

We now describe two experiments that are used to obtain $\mathbf{u}^j\,, j = 1, 2$, which in turn are used in Eq. (38.a, b). The first experiment concerns the cylinder with the inclusion being pulled in one direction while, at the same time, being compressed in the other direction, as illustrated in Fig. 1. The resultant forces on both sides have the same intensity τ_1. The boundary conditions for this experiment are given below.

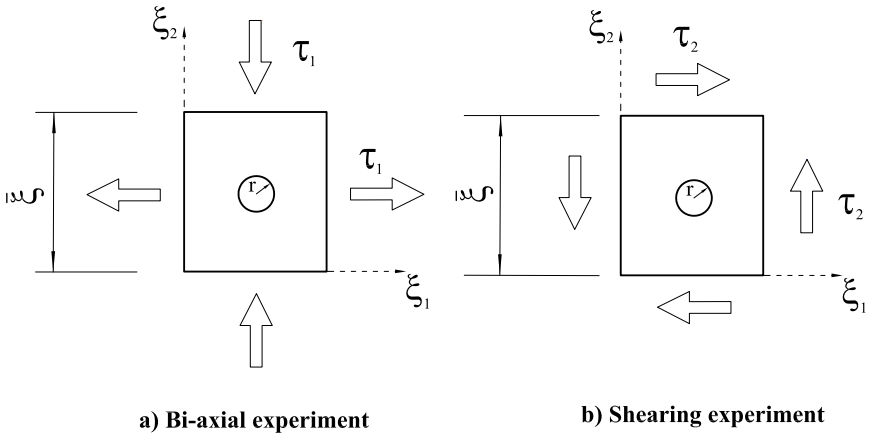

a) Bi-axial experiment **b) Shearing experiment**

Figure 1: Experiments for the determination of μ.

a) Vertical sides:

$$u_1(0, \xi_2) = 0\,, \qquad u_1(\bar{\xi}, \xi_2) = \bar{\varepsilon}_1\,\bar{\xi}\,, \tag{40}$$

$$(\mathbf{e}_2 \cdot \mathbf{T}\,\mathbf{e}_1)(0, \xi_2) = (\mathbf{e}_2 \cdot \mathbf{T}\,\mathbf{e}_1)(\bar{\xi}, \xi_2) = 0\,, \tag{41}$$

where $\bar{\varepsilon}_1 = 0.01$.

b) Horizontal sides:

$$u_2(\xi_1, 0) = 0\,, \qquad u_2(\xi_1, \bar{\xi}) = -\bar{\varepsilon}_1\,\bar{\xi}\,, \tag{42}$$

$$(\mathbf{e}_1 \cdot \mathbf{T}\,\mathbf{e}_2)(\xi_1, 0) = (\mathbf{e}_1 \cdot \mathbf{T}\,\mathbf{e}_2)(\xi_1, \bar{\xi}) = 0\,. \tag{43}$$

In the second experiment, the lateral sides of the cylinder with the inclusion are submitted to a displacement field given by the expressions below.

a) Vertical sides:

$$u_1(0,\xi_2) = u_1(\bar{\xi},\xi_2) = 2\,\bar{\varepsilon}_2\,\xi_2\,, \tag{44}$$

$$u_2(0,\xi_2) = u_2(\bar{\xi},\xi_2) = 0\,, \tag{45}$$

where $\bar{\varepsilon}_2 = 0.01$.

b) Horizontal sides:

$$u_1(\xi_1,0) = 0\,, \qquad u_1(\xi_1,\bar{\xi}) = 2\,\bar{\varepsilon}_2\,\bar{\xi}\,, \tag{46}$$

$$u_2(\xi_1,0) = u_2(\xi_1,\bar{\xi}) = 0\,. \tag{47}$$

If the cylinder is homogeneous, i.e., if $C_R = 1$ in Eq. (39.d), the solution of the direct problem associated to the second experiment is homogeneous and given by $u_1(\xi_1,\xi_2) = 2\,\bar{\varepsilon}_2\,\xi_2$, $u_2(\xi_1,\xi_2) = 0$. In this case, the normal components of stress acting on the sides of the cylinder vanish and we only have the resultant forces of intensity τ_2 depicted in Fig. 1.b. If the cylinder is non-homogeneous, i.e., if $C_R \neq 1$ in Eq. (39.d), the solution of the associated direct problem is not homogeneous and yields normal components of stress on the sides of the cylinder that, in general, do not vanish. For all the cases considered in this work, it was verified that these normal components are much smaller than the tangential components of stress acting on these sides. Even though the resultant forces due to these small values of normal stress are not depicted in Fig. 1.b, they were considered in the formulation of the inverse problem.

Approximate solutions of the discrete direct problems associated to the experiments described above were obtained with the finite element package *ANSYS 5.5*[2]. The formulation used by this package is based on the discrete formulation described in Section 3.1.

As discussed in Section 3.2, we use these approximate solutions in the formulation of the discrete inverse problem. We then solve this problem to obtain an approximate field for the shear elastic modulus μ. For this, we have implemented a finite element program that is based on the discrete formulation given by Eq. (37) thru Eq. (38).

In the next two figures we show sequences of frames that use color maps to represent the distribution of the shear elastic modulus in the cylinder containing the centered inclusion. Each frame has its own color map, which corresponds to a range of values for μ. The smallest and largest values of μ correspond to the colors at, respectively, the bottom and the top of the color map. The frames on the upper left corner in both figures contain exact values of μ and are used as reference frames to be compared with the other five frames. These five frames are obtained from different finite element meshes, which are presented in Table 1. Observe from this table that we are considering an increasing number of both nodes and elements.

Table 1: Finite element meshes for the cylinder with a centered inclusion.

mesh	Number of nodes	Number of elements
1	803	738
2	1016	951
3	1148	1083
4	1380	1315
5	1544	1479

[2] *ANSYS 5.5* is proprietay software of Anys Inc., PA, USA.

In figures 2 and 3 we consider the cases $C_R = 0$[3] and $C_R = 6$, respectively. Comparing the reference frame (a) in each figure with the other five frames of the same figure and observing the values in the corresponding legend, we note that μ_h, defined by Eq. (36.a), converges to μ as the mesh is refined. In both cases, $\mu_h \to 36$ kPa everywhere inside the matrix. Inside the inclusions, we see from Fig. 2 that $\mu_h \to 0$ kPa and from Fig. 3 that $\mu_h \to 216$ kPa.

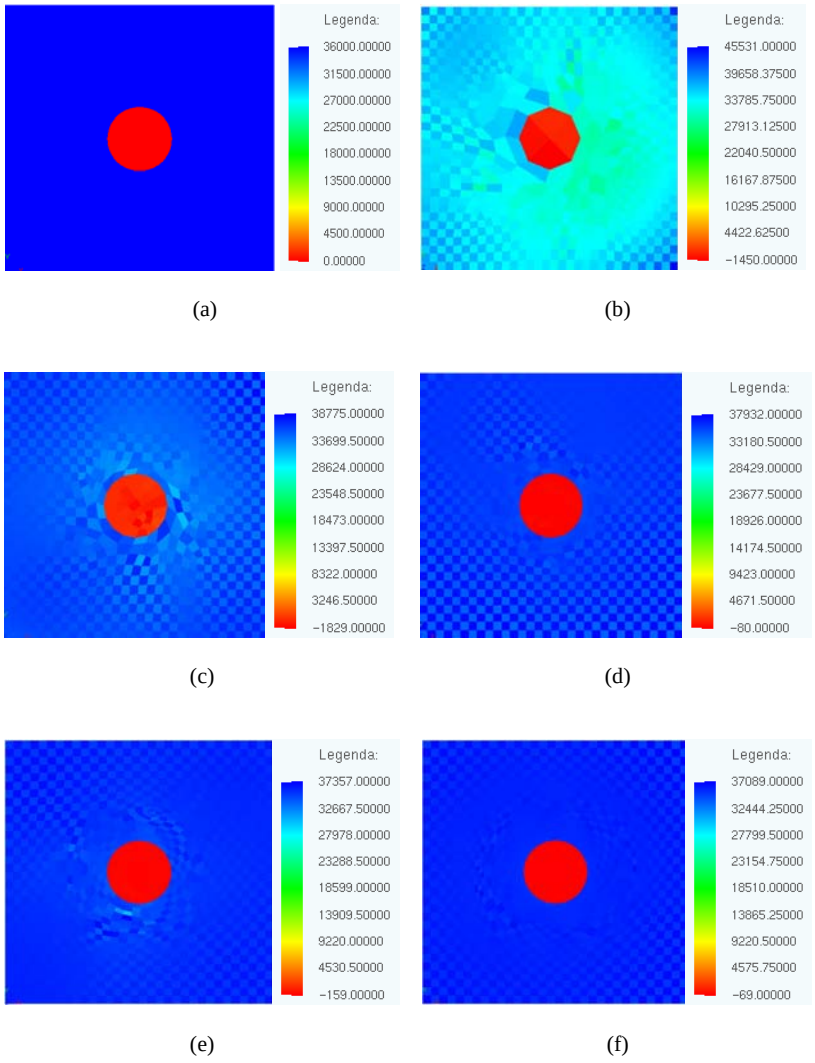

Figure 2: Reconstruction of μ [Pa] in a cylinder containing a centered hole, $C_R = 0$. (a) Reference frame; (b) - (f) Frames obtained from meshes in Table 1.

Next, we compare our methodology of reconstruction of μ with the methodology presented by Park and Maniatty (2006). These authors present a direct inversion approach for reconstructing μ in a nearly incompressible, isotropic, and linearly elastic solid from dynamic measurements of the interior displacement field during time harmonic excitation. The authors use a finite element methodology to find approximate solutions to the governing equations, which does not use boundary conditions. Here, however, they simulate numerically only one experiment, instead of two in our case, in order to obtain the displacement field. In particular, they consider the cylinder with the centered inclusion presented above. The cylinder is in a state of

[3]Because of numerical difficulties experienced during the numerical simulation of the discrete direct problem with *ANSYS 5.5*, we used $C_R = 10^{-25}$ and $\nu_I = 0.3$, instead of $C_R = 0$ and $\nu_I = 0.5$.

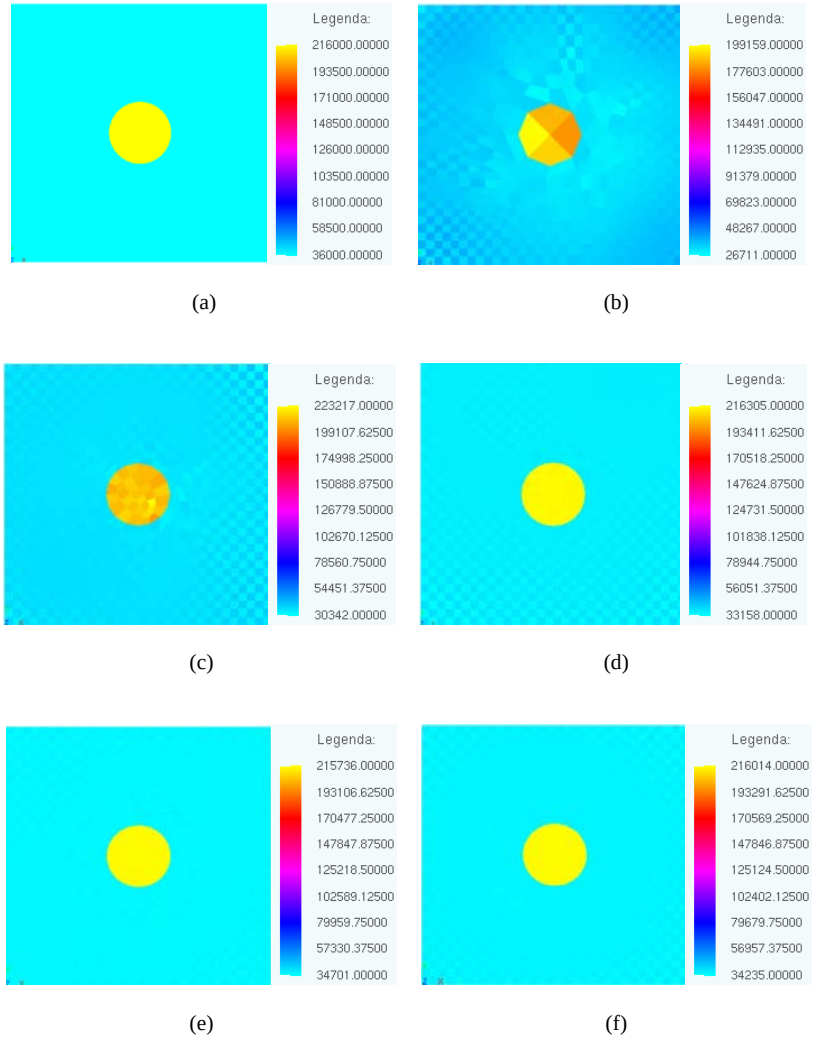

Figure 3: Reconstruction of μ [Pa] in a cylinder containing a centered inclusion with $C_R = 6$. (a) Reference frame; (b) - (f) Frames obtained from meshes in Table 1.

plane strain parallel to its bases. One of its lateral sides is kept fixed while the opposite side is submitted to a horizontal excitation of 150 MHz with an amplitude of 1 mm. The other two lateral sides are traction free. The matrix has the same shear elastic modulus as ours, given by Eq. (39.b), and a slightly smaller Poisson ratio, given by $\nu = 0.499992$, which is the same one for the inclusion.

Park and Maniatty (2006) present a table containing some results from their computations. In particular, they present values for the per cent average error in the reconstructed shear modulus, which is defined by $E_\mu = 100\,\Delta\mu/\bar{\mu}$. In this expression, $\Delta\mu = \sqrt{\int\limits_{\mathcal{B}} (\mu_h - \mu)^2\, d\,\mathbf{x}\big/ A_{\mathcal{B}}}$, where $A_{\mathcal{B}} \equiv \bar{\xi}^2$ is the area of the square cross section and μ_h is their finite element approximation for the known distribution μ, and $\bar{\mu} = \sqrt{\int\limits_{\mathcal{B}} \mu_h^2\, d\,\mathbf{x}\big/ A_{\mathcal{B}}}$. They also present values for the average reconstructed shear modulus of the inclusion, which we infer[4] from their paper that it is given by $\bar{\mu}_I = \int\limits_{\mathcal{B}_I} \mu_h\, d\,\mathbf{x}\big/ A_{\mathcal{B}_I}$, where $A_{\mathcal{B}_I} = \pi\, r^2$ is the area of the circular cross section. For

[4]We use the expression (20) in Park and Maniatty (2006).

the case of a circular inclusion of radius $r = 6$ mm and $C_R = 6$, these values are $E_\mu = 21.91\%$ and $\bar{\mu}_I = 191.2$ kPa.

Next, we adapt the authors dynamic experiment to a static experiment, so that we can use it in our simulations. For this, we consider that the cylinder is in equilibrium, fixed in one lateral side, and subjected to a horizontal displacement of 1 mm on the opposite lateral side. The conditions on the other lateral sides are the same as in Park and Maniatty (2006).

The additional experiment needed in our simulations consists of compressing the lateral sides of the cylinder through rigid frictionless platens while keeping the other two lateral sides traction free.

The finite element mesh used in our simulation is mesh 5 in Table 1. We have verified that $\max_{x_i \in \mathcal{B}_I} |\mu_i - \mu(\mathbf{x}_i)| \cong 2.1kPa$, where $n = 1544$ and we recall from Section 3. that μ_i is the approximate value of μ at the node $\mathbf{x}_i$. This difference corresponds to $\mu_i \cong 213.9$ kPa for a node $\mathbf{x}_i$ located inside the inclusion. Comparing this value with $\bar{\mu}_I = 191.2$ kPa of Park and Maniatty (2006), we see that our methodology yields a much better approximation to μ than the methodology proposed by those authors.

5. Conclusion

We have presented a numerical procedure for the determination of the shear elastic modulus μ of a linearly elastic, isotropic, and incompressible solid in a state of plane strain. It is assumed that two linearly independent displacement fields are known inside the body from two distinct experiments and that resultant forces are known on complementary parts of the boundary of the solid. We have presented numerical results that are in very good agreement with analytical results. When compared to another numerical procedure presented in the literature, (Park and Maniatty, 2006), our procedure yields more accurate results. Our numerical procedure has great potential of application in Medical Physics; especially, in the detection of tumors inside healthy biological tissues and in the identification of different tissues in parts of the human body. It also has the potential of being applied in all branches of engineering requiring non-destructive evaluation of the interior of a solid body in a state of plane strain.

Acknowledgements

The authors wish to acknowledge CAPES (Coordination for the Improvement of High Education Personnel) for its support of this research.

REFERENCES

Aguiar, A. R. & Fosdick, R. L., 2000. A singular problem in incompressible nonlinear elastostatics. *Mathematical Models and Methods in Applied Sciences*, vol. 10, pp. 1181–1207.

Barbone, P. E. & Gokhale, N. H., 2004. Elastic modulus imaging: on the uniqueness and nonuniqueness of the elastography inverse problem in two dimensions. *Inverse Problems*, vol. 20, pp. 283–296.

Fung, Y. C., 2004. *Biomechanics: Mechanical Properties of Living Tissues*. New York: Springer, 2 edition.

Golub, G. H. & van Loan, C. F., 1996. *Matrix Computations*. Baltimore: The John Hopkins University Press, 3 edition.

Krouskop, T. A., Wheeler, T. M., Kallel, F., Garra, B. S., & Hall, T., 1998. Elastic moduli of breast and prostate tissues under compression. *Ultrason. Imaging*, vol. 20, pp. 260–274.

Liu, H. T., L.Z.Sun, G.Wang, & Vannier, M. W., 2003. Analytic modeling of breast elastography. *Medical Physics*, vol. 30, n. 9, pp. 2340–2349.

McLaughlin & Yoon, J. R., 2004. Unique identifability of elastic parameters from time-dependent interior displacement measurement. *Inverse Problems*, vol. 20, pp. 25–45.

Mridha, M. & Ödman, S., 1986. Noninvasive method for the assessment of subcutaneous edema. *Med. Biol. Eng. Comput.*, vol. 24, n. 4, pp. 393–398.

Ophir, J., Cspedes, I., Ponnekanti, H., Yadi, Y., & Li, X., 1991. Elastography: a quantitative method for imaging the elasticity of biological tissues. *Ultrason. Imaging*, vol. 13, pp. 111–134.

Ophir, J., Kallel, F., Varghese, T., Konofagou, E., Alam, S. K., Krouskop, T., Garra, B., & Righetti, R., 2001. Optical and acoustical imaging of biological media: Elastography. *C.R.Acad Sci. Paris-Applied Physics (Biophysics)*, vol. 2, n. series IV, pp. 1193–1212.

Park, E. & Maniatty, A. M., 2006. Shear modulus reconstruction in dynamic elastography: time harmonic case. *Physics in Medicine and Biology*, vol. 51, pp. 3697–3721.

Sarvazyan, A., 1993. Shear acoustic properties of soft biological tissues in medical diagnostics. *The Journal of the Acoustical Society of America, ASA*, vol. 93, n. 4, pp. 2329–2330.